9th ANKARA INTERNATIONAL AEROSPACE CONFERENCE AIAC-2017-147
20-22 September 2017 - METU, Ankara TURKEY

EXPERIMENTAL INVESTIGATIONS ON PARTICLE EROSION BEHAVIOR OF AA 6061 ALLOY

Doğan Acar [1] , Dursun Meriç [2], Ali İhsan Budur [3] , Recep Gümrük [4] , Hasan Sofuoğlu [5], Hasan Gedikli [6] , Ömer Necati Cora [7]

Karadeniz Technical University
Trabzon, Turkey

ABSTRACT

Solid particle erosion behavior of AA 6061 aluminum alloy was evaluated using a recently developed erosion wear test system. Wear tests were performed under different impact angles (20°, 30°, 45°, 60°, 90°) and velocities (74, 90, 150, 195 m/s) at ambient temperature. Alumina particles with 50 µm in dimension were used as erodent. Results showed that higher the impact velocity the higher the erosion rate is obtained. On the other hand, the highest erosion rate was recorded for the impact angle of 20°. Optical microscopy images revealed that several mechanisms such as plastic deformation and scratching involved in erosion behavior.

INTRODUCTION

Solid particle erosion is one of the major reasons leading large financial losses and service interruptions in aviation industry. Gas turbines blades, fuel tanks, ammunition, compressors of helicopters and aircrafts are among the components affected by solid particle erosion. A structural part called *erosion shield* is used to minimize erosion in helicopter rotor blades. The major goal of this application is to minimize (prevent if possible) damage on composite structured main rotor blade, especially during take-off and landing. The standard erosion tests [e.g., ASTM G76-13, 2013; ASTM F1864-16, 2010] are not capable of reflecting the take-off, landing conditions, and therefore are not regarded as appropriate for testing erosion performance of erosion shields. Therefore, a dedicated testing method was developed and standardized [MIL-STD-3033, 2012]. According to this standard, erodent particles must be angular-shaped quartz sand within the dimension range of 240-550 µm while the impact velocity of erodent particles is recommended to be 225 ± 10.6 m/s (730 ± 30 ft/s). A test system that is capable of performing erosion tests per abovementioned standards was developed by authors within the scope of this study (Figure 1).

[1] GRA, KTÜ Department of Mechanical Engineering, email: dgnacar@ktu.edu.tr
[2] Lecturer, KTÜ Abdullah Kanca Vocational School, email: dmeric@ktu.edu.tr
[3] Lecturer, KTÜ Arsin Vocational School, email: ali.budur@ktu.edu.tr
[4] Assoc. Prof., KTÜ Department of Mechanical Engineering, email: rgumruk@ktu.edu.tr
[5] Prof., KTÜ Department of Mechanical Engineering, email: sofuoglu@ktu.edu.tr
[6] Assoc. Prof., KTÜ Department of Mechanical Engineering, email: hgedikli@ktu.edu.tr
[7] Assist. Prof., KTÜ Department of Mechanical Engineering, email: oncora@ktu.edu.tr

The literature is abundant in terms of investigating the individual effects of parameters such as temperature, impact velocity, erodent particle size, impact angle and target material on the wear performance of materials [Gat and Tabakoff, 1978; Andrews and Field, 1982; Bousser et al., 2013; Sundararajan and Roy 1997; Islam and Farhat, 2014]. The combination of all these parameters induce relatively complex conditions that requires cumbersome investigations [Evans and Wilshaw, 1976; Head and Harr, 1970; Dhar et al., 2005; Stack and Pungwiwat, 2002]. Among those parameters, impact velocity and angle has critical importance [Okonkwo et al., 2015].

Lindsey et al. [1999] investigated the erosion rate of 70-30 brass and Fe-C martensite alloys at different impact velocities. They showed that erosion rate is dependent on impact velocity. Besides, it was observed that martensite alloys were eroded by cracking mechanism while brass was eroded by plastic deformation. [Stackwick and Batchelor, 2011] reported that erosion rate increases with increasing impact angle and maximum rate was obtained at 90° impact angle. Effect of impact angle and velocity on pipe lines produced with AISI 1018 was investigated by [Okonkwo et al., 2004]. At the impact angle of 90°, ploughing was the effective erosion mechanism, as for low impact velocities micro-cutting was major erosion mechanism. Besides, it was reported that increasing impact velocity resulted in increase for erosion rate and mass loss of AISI 1018. [Matsumara et al., 1991] performed erosion tests on SS 304 stainless steel to investigate the effect of different impact angles on the erosion mechanism using silica sand particles. Maximum erosion rate was obtained between 30°-50° impact angles. [Finnie et al., 1960] reported that the maximum erosion rate for ductile materials was found at 15°- 40° impact angles.

In erosion phenomenon, it is well-known that erosion mechanism come into prominence when erodent particles impact the target material. There is quite a few literature for the erosion mechanisms of steel materials [Finnie, 1958; Forder et al., 1998; Desale et al., 2006; Al-Bukhaiti et al., 2007; Al-Bukhaiti et al., 2009; Forero et al., 2014]. Erosion mechanism is regarded as a complicated phenomenon; and it has not been completely understood yet". Al-Bukhaiti et al. [2007] observed different erosion mechanisms (micro-cutting, scratching which lead to shear lip, carbide fracture and chips) in the tests they performed with AISI 1017 and cast iron. In another study, ploughing, fracture and cutting mechanisms were noted to be effective on erosion behavior of API X42 steel which was eroded with aluminum oxide particles [Islam et al, 2014]. In another study, [Okonkwo et al., 2014] investigated the normal impact angle erosion mechanisms of AISI 1018 and API X42 steels. Researchers found that erosion mechanism differs depending on impact velocity and target material.

In the current study, solid particle erosion behavior of AA 6061 aluminum alloy was evaluated as a candidate erosion shield material by means of MIL-STD 3030 standardized testing. The results were compared with the performance of AISI 1020 which is standard target material cited in ASTM-G76.

EXPERIMENTAL

Test System and Calibration

Schematic drawing and picture of developed test system is shown in Figure 1. The test system is composed of three main sections. The first section contains an air compressor with a pressure capacity of 40 bar and a reservoir tank for pressurized air. Second section includes a pressure conditioning tank and dust (erodent alumina particles) feeding system (Figure 2-a, b). In this section, the air is conditioned to the predetermined pressure values to achieve necessary velocities for erodents. In the last section, there is a test cabin covering linear moving platform actuated by a step motor. Test specimens are mounted on a platform which can move up, and down as well as left and right (Figure 2-c). Test system is capable of providing different impact angles and nozzle distances. Whole test system is controlled with control panel.

The test system devised and constructed was first used to determine the wear performance of AISI 1020 steel per ASTM G76-13 standard. AISI 1020 is the reference material in the

standard, and it was used for calibration purposes. Test results showed quite a well agreement with the ones reported in ASTM G76-13 (Figure 3). Following the calibration, erosion tests were carried out for AA 6061 aluminum alloy.

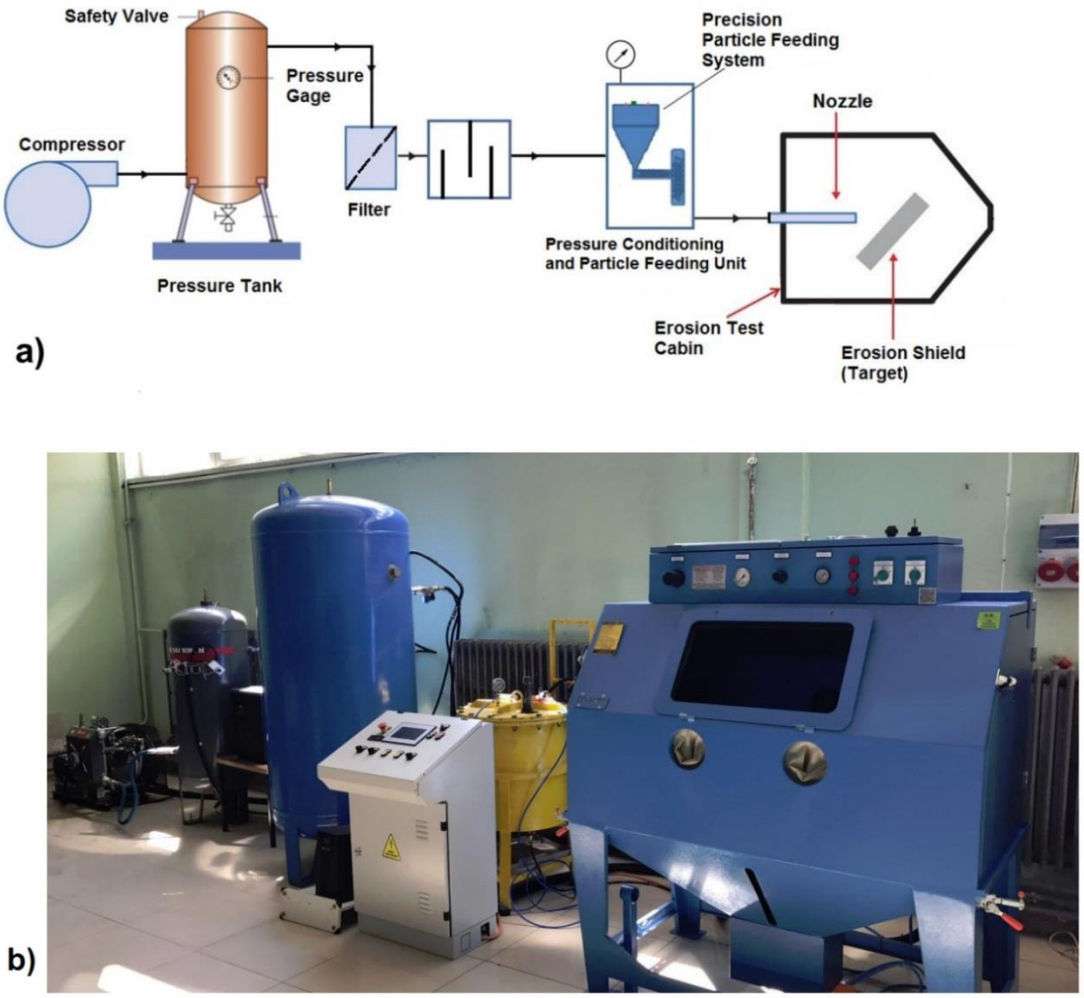

Figure 1. Solid particle erosion test system developed, a) Schematic of test system, b) Actual photo of test system

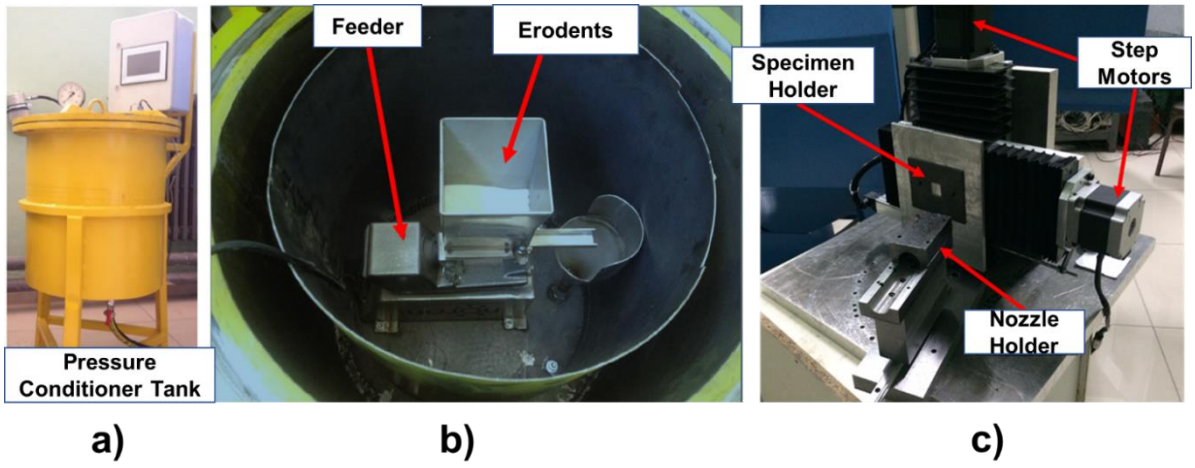

Figure 2. Details of the test system, a) Pressure conditioning tank, b) Inside the pressure conditioning, c) Inside the test cabin: platform that specimens mounted on

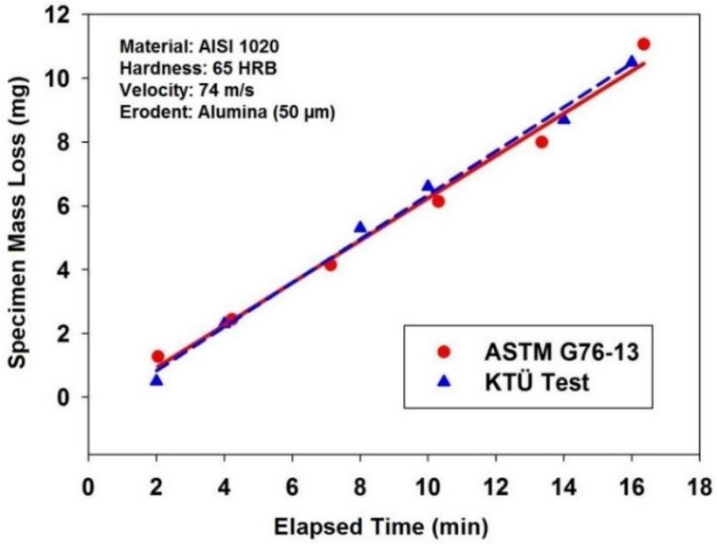

Figure 3. Comparison of erosion tests on AISI 1020 with ASTM G76-13 for calibration of solid particle erosion test system

Erosion Tests

AA 6061 aluminum sheet metal alloy with 0.5 mm thickness was the material of interest in erosion tests. The chemical composition of AA 6061 is given in Table 1. AA 6061 alloy is known to have good mechanical properties as well as decent weldability and good corrosion resistance. It is preferred in aircraft fittings, wings, and fuselages of experimental aircrafts. Erosion test samples were cut into 25x25 mm dimension by means of electric discharge machining (EDM). Grinding through a series of abrasive papers down to 400 grit was performed to achieve smooth surface finish. Recommended surface roughness is 1 µm by the standards and roughness measurements were obtained with MahrSurf M300 portable surface roughness measurement device. Polished specimens were cleaned in trichloro-ethylene solution ultrasonically before and after the erosion experiments. In pursuit of cleaning processes, each specimen was weighted with 1 mg precision to evaluate the mass loss. Vickers hardness measurements were performed using Struers Duramin with indentation load of 1.92 N for 10 seconds. Average hardness value of 110±2 HV was obtained

Specimens, then were mounted onto the test system and subjected to solid particle erosion testing. Different impact angles (20°, 30°, 45°, 60°, 90°) and velocities (74, 90, 150, 195 m/s) were experimented. Different impact velocities were realized by implementing different pressure values namely, 300, 680, 2100 and 4000 mbar for velocities of 74, 100, 150 and 195 m/s, respectively. Before each test, erodent particle velocity was measured by means of double-disk method which its detail can be found in literature [Ruff and Ives., 1975]. As erodent, alumina particles with a nominal dimension of 50 µm were used. Each test conditions were repeated at least three times to address repeatability.

RESULTS and DISCUSSIONS

Figure 4 shows the tested samples and erosion crater and tracks observed at different impact angles and velocities. It is clearly seen that as the impact angle increases the wear scar in elliptical form converts to circular one (e.g. at 60° and 90°).

After experiments completed, surface scanning of test specimens was performed with Nanofocus (µscan) 3D non-contact laser optical profilometer. Surface roughness and

topology, as well as sectional profiles for craters were acquired. As it can be seen from Figure 4, the shape of the erosion crater turns into a circular structure from elliptical one as the impact angle increases. Besides, maximum depth value for craters increases with the increasing impact angle.

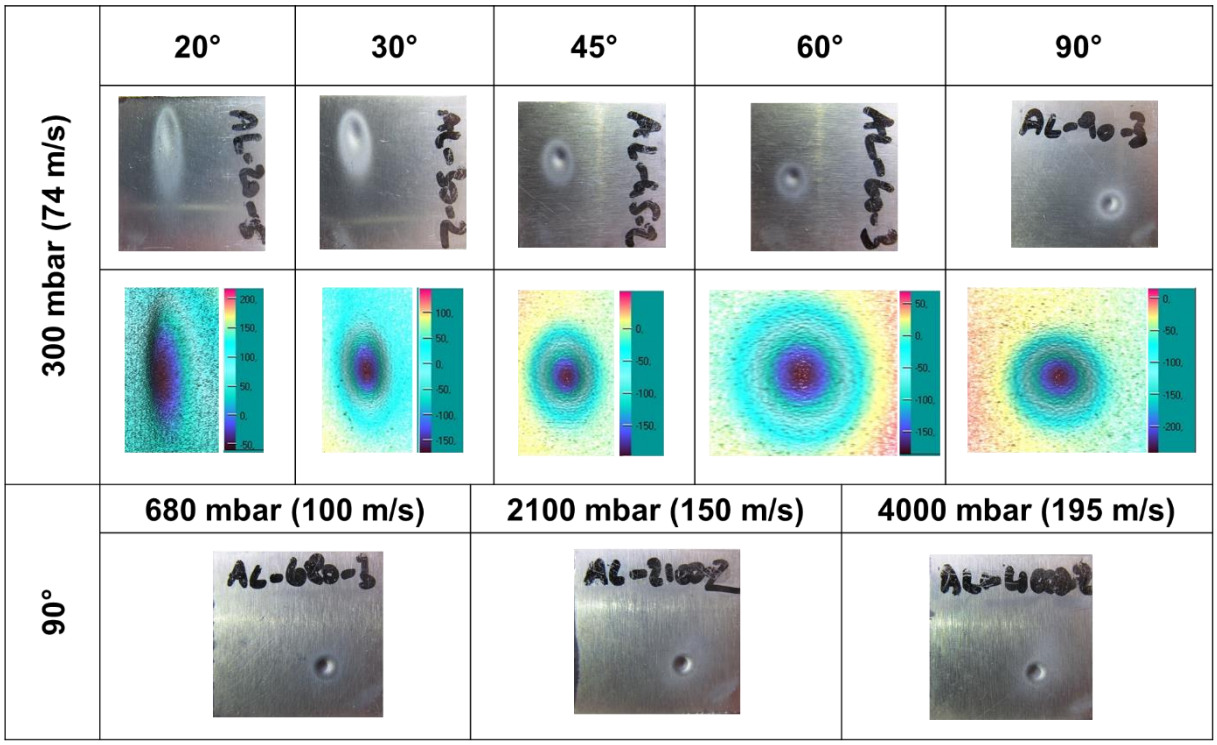

Figure 4. Erosion crater and tracks on tested specimens obtained at different impact angles and velocities

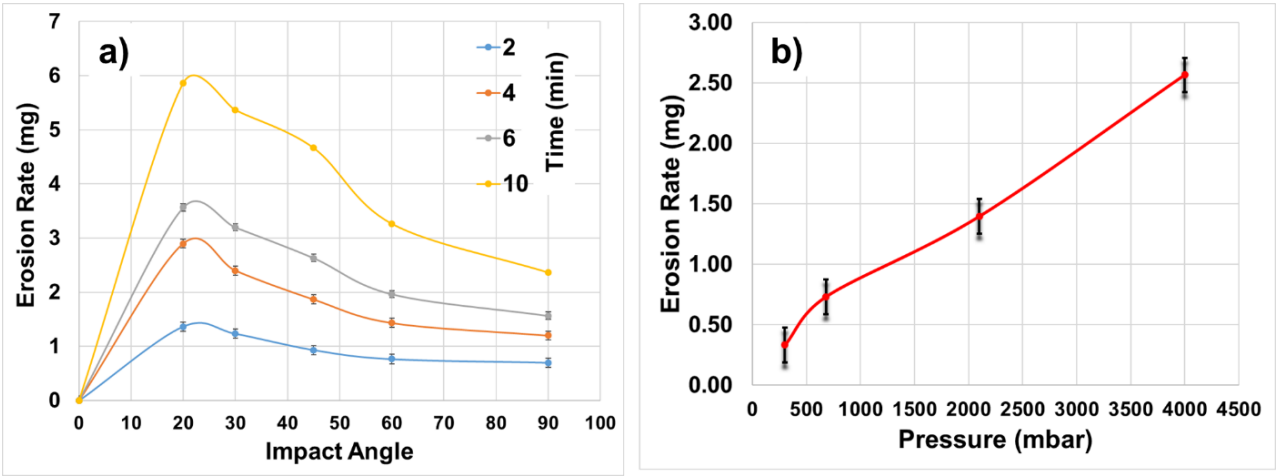

Figure 5. Erosion rates for AA 6061 alloy, a) as a function of impact angles obtained at 74 m/s, b) at different particles speeds (300 mbar = 74 m/s; 680 mbar = 100 m/s, 2100 mbar = 150 m/s, 4000 mbar=195 m/s)

Effect of Impact Angle and Velocity

Figure 5-a shows the erosion rate of AA 6061 aluminum alloy as a function of erodent impact angle for different test durations and with a 74 m/s erodent particle speed. As it can easily be noticed, maximum erosion rate was measured at impact angle of 20°. As erosion is mainly due to shear forces, highest erosion rates were obtained at lower impact angles (e.g. 20°).

This is the result of higher tangential forces and lower normal component of stress of the impacting particles at the lower impingement angles [Khayatan et al., 2017]. This particular mode of erosion is named as ductile erosion [A. Patnaik et al., 2010]. As a result, lower impingement angles cause more sliding and less penetration. Figure 5-b, on the other hand, shows the variation of erosion rate as a function of erodents' velocity. As expected, higher the impact velocity, the higher erosion rate was recorded. In other words, higher kinetic energy of erodents resulted in higher erosion rates. It was also noted that the relation between the erosion rate and particle speed is almost linear.

The results obtained in current study were also compared witth the ones obtained by Yerramareddy and Bahadur. They tested Ti6-Al-4V alloy samples which were air cooled from 940˚C using a horizontal sand-blast test rig [Yerramareddy and Bahadur, 1991]. In their tests, silicon carbide particles 125 μm in nominal dimensions (120 grit) were used as erodents. The impingement velocity of particles was set to 55 m/s. Even though the test conditions are not same with the current study, comparison of erosion rates with respect to impact angle is provided in Figure 6. It is observed that the erosion rates at oblique impact condition (90˚) are quite close yet the maximum erosion rate for AA 6061 was almost half of the one obtained for Ti-6Al-4V. In addition, different from current study, maximum erosion rate was obtained at 30˚ for Ti-6Al-4V.

Microscopic Examinations

Optical microscopy was used to examine the eroded surfaces so the erosion mechanism. Optical micrographs given in Figure 7, reveal the different erosion mechanisms for the tests performed at different impact angles. Plastic deformation and scratching are the major erosion mechanisms where some micro-cutting mechanisms are also observed. While plastic deformation is observed all impact angles, it was observed that scratching loses its effect with increasing impact angle. This phenomenon lead us that both shear and normal stresses are effective at low impact angles while normal stresses are more effective at higher impact velocities.

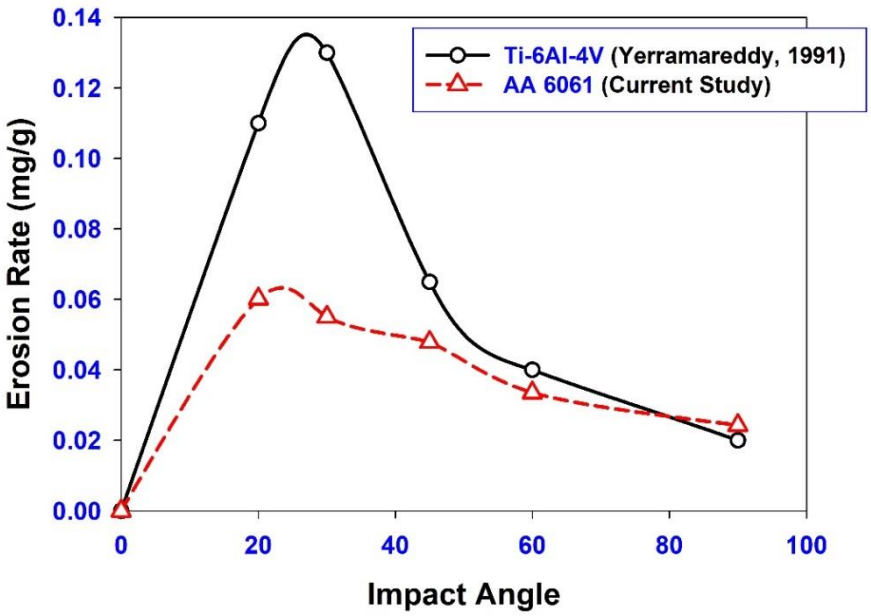

Figure 6. Comparison of erosion rate-impact angle behavior of AA 6061 and Ti-6Al-4V alloys

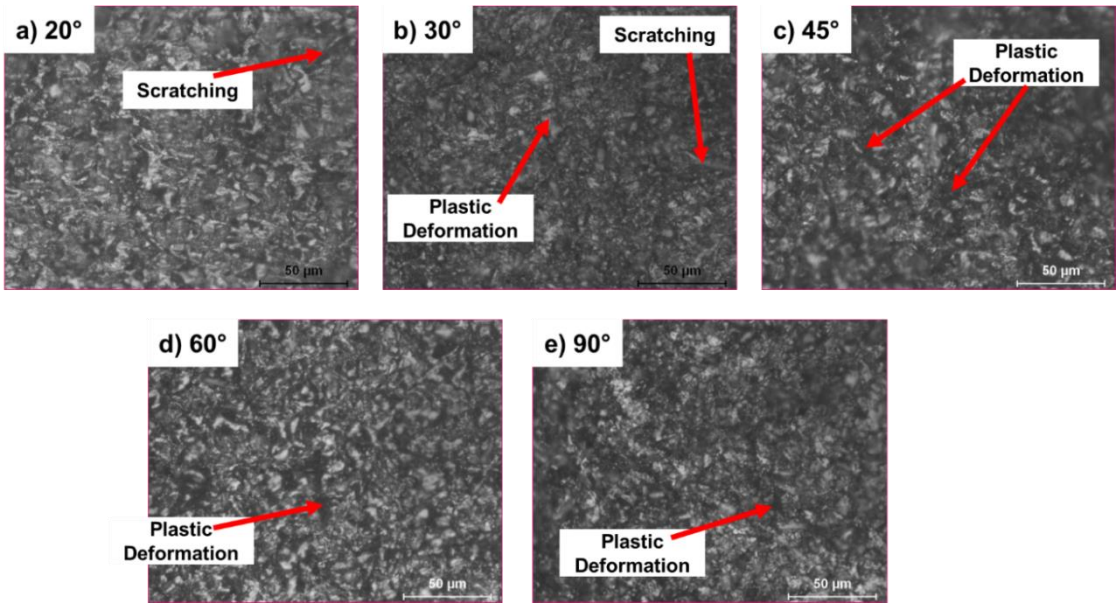

Figure 7. Optical micrographs obtained from the test sample surfaces for different impact angles, a) 20˚, b) 35˚, c) 45˚, d) 60˚, e) 90˚

Worn surfaces were also scrutinized by means of non-contact laser profilometer. The section profile that passes through the deepest point of the crater was extracted for each sample. As an example, Figure 8 shows the section profile of the samples tested with 74 m/s impact velocity, and 20° impact angle. Comparison of maximum crater depths with respect to impact angle and velocity are provided in Figure 8. It was observed that crater depth increases with the increasing impact angle except for the 60˚ case. Maximum crater depth of 247 µm was obtained at 90° impact angle (Figure 8a). Effect of impact velocity on the crater depth comparison was based on the tests performed with at 90° impact angle (Figure 9-b). It is seen that up to 150 m/s, the crater depth increases with the increasing impact velocity whereas lower crater depth was obtained at impact velocity of 195 m/s. Even though it needs further investigation it is assumed that above certain impact velocity, the erodent particles hardens the surface (e.g. plastic deformation by compressive stress) rather than resulting in wear.

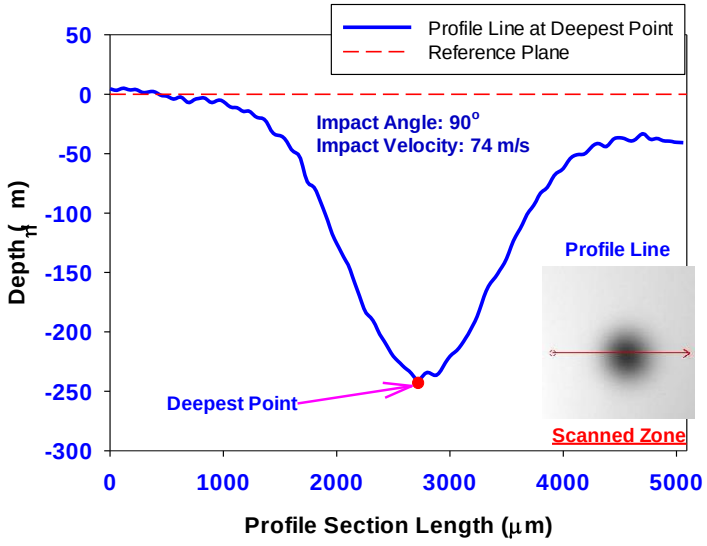

Figure 8. An example of section profile for specimen tested at 20° impact angle and 74 m/s impact velocity for its deepest point

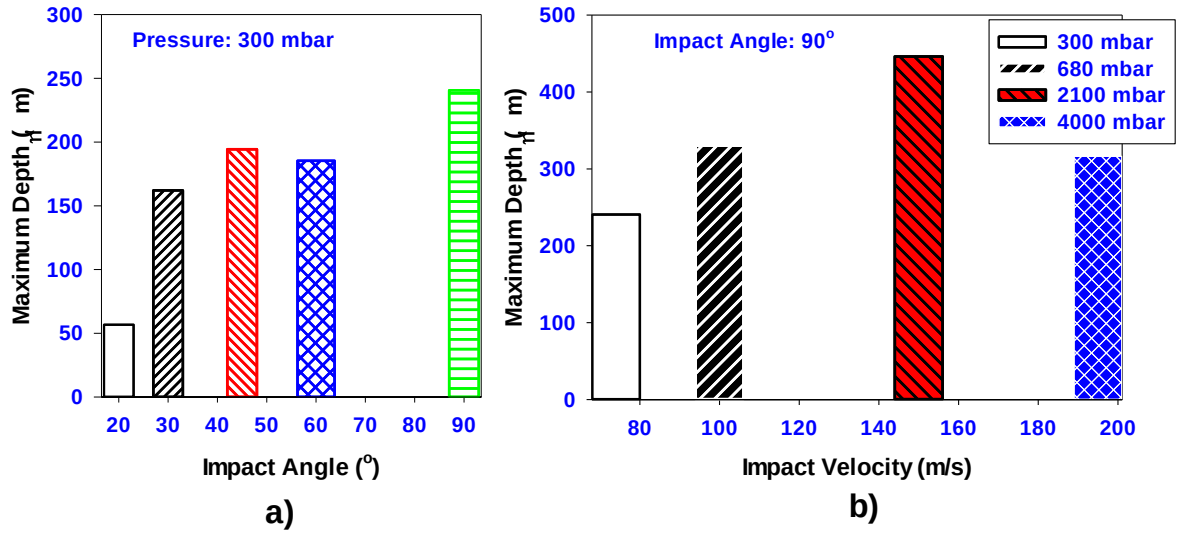

Figure 9. Surface scan results: Effect of impact angle, b) impact velocity on maximum depth occurred in the erosion crater

CONCLUSIONS

AA 6061 aluminum alloy with 0.5 mm thickness was subjected to solid particle erosion tests using an in-house developed erosion wear test system to assess whether AA 6061 is a candidate material for replacing conventional erosion shield materials. To this goal, erosion tests were performed at different impact angles (20°, 30°, 45°, 60° and 90°) and velocities (74, 100, 150 and 195 m/s). Main outcomes from this research are summarized as follows:

- The highest erosion rate for AA 6061 aluminum alloy was recorded at 20° impact angle.
- With increasing impact velocity, the erosion rate of AA 6061 also increased due to higher kinetic energy of erodent particles, as expected.
- Although, scratching and plastic deformation are the major observed erosion mechanisms, scratching mechanism loses its dominance as the impact angle increases.
- Increasing impact angle, shape of the erosion crater turns from elliptical shape to circular one.
- Erosion crater maximum depth, is achieved at 90° impact angle and for impact velocity of 150 m/s.
- Maximum erosion rate for AA 6061 aluminum alloy was noted at 20° impact angle.
- Even though it needs further investigations, AA 6061 can be alternative to current erosion shield materials.

ACKNOWLEDGEMENT

This study was partially supported by Turkish Aerospace Industries (TAI) – Rotary Wing Technology Center project #: DKTM-2015/03 & contract #: 201500439.

References

Al-Bukhaiti M., Ahmed S., Badran F. and Emara K., (2007) Effect of impingement angle on slurry erosion behaviour and mechanisms of 1017 steel and high-chromium white cast iron, Wear, Vol. 262(9), p: 1187-1198.

Al-Bukhaiti M., Emara K. and Ahmed S., (2009) Fractal Characterization of Slurry Eroded Surfaces at Different Impact Angles, Journal of Tribology, Vol. 131(3), p: 031601.

Andrews D. and Field J., (1982) *Temperature dependence of the impact response of copper: erosion by melting*, Journal of Physics D: Applied Physics, Vol. 15(11), p: 2357.

ASTM G76-13, (2013) *Standard Test Method for Conducting Erosion Tests by Solid Particle Impingement Using Gas Jets*, ASTM International, West Conshohocken, PA, USA.

ASTM F1864-05 (2010) *Dust Erosion Resistance of Optical and Infrared Transparent Materials and Coatings*, ASTM International, West Conshohocken, PA, USA.

Bousser E., Martinu L. and Klemberg-Sapieha J. (2013) *Effect of erodent properties on the solid particle erosion mechanisms of brittle materials*, Journal of Materials Science, Vol. 48(16), p: 5543-5558.

Desale G. R., Gandhi B. K. and Jain S., (2006) Effect of erodent properties on erosion wear of ductile type materials, Wear, Vol. 261(7), p: 914-921.

Dhar S., Krajac T., Ciampini D. and Papini M. (2005*) Erosion mechanisms due to impact of single angular particles*, Wear, Vol. 258(1), p: 567-579.

Evans A. and Wilshaw T. R. (1976*) Quasi-static solid particle damage in brittle solids—I. Observations analysis and implications*, Acta Metallurgica, Vol. 24(10), p: 939-956.

Finnie I., (1958) The mechanism of erosion of ductile metals, 3rd US National Congress of Applied Mechanics.

Finnie I., 1960. Erosion of surfaces by solid particles, Wear, Vol. 3(2), p: 87-103.

Forder A., Thew M. and Harrison D., (1998) A numerical investigation of solid particle erosion experienced within oilfield control valves, Wear, Vol. 216(2), p: 184-193.

Forero A., Núñez M. and Bott I., (2014) Analysis of the corrosion scales formed on API 5L X70 and X80 steel pipe in the presence of CO2, Materials Research, Vol. 17(2), p: 461-471.

Khayatan N., Ghasemi H.M. and Abewdini M., (2017) Synergestic erosion-corrosion behavior of commercially pure titanium at various impingement angles, Wear, Vol. 380-381, p: 154-162.

Levin, B.F., Vecchio, K.S., DuPont, J.N. and Marder, A.R., (1990) Modeling Solid-Particle Erosion of Ductile Alloys, Metallurgical and Materials Transactions A, Vol. 30A, p: 1763-1774.

MIL-STD-3033 (2012) *Particle/Sand Erosion Testing for Rotor Blade Protective Materials*, U.S. Army Research Laboratory, Weapons and Materials Research Directorate, Materials Manufacturing Technology Branch, Specification and Standards Office, Aberdeen Proving Ground, MD, USA.

Okonkwo P.C., Mohamed A.M.A. (2014) *Erosion Mechanisms of API X42 and AISI 1018 Steel Materials at Normal Impact Angle*, International Journal of Engineering Science and Innovative Technology, Vol. 3(5), p: 402-407.

Okonkwo P.C., Mohamed A.M.A. and Ahmed E. (2015) *Influence of particle velocities and impact angles on the erosion mechanisms of AISI 1018 steel*, Advanced Material Letters, Vol. 6(7), p: 653-659.

Patnik A., Satapathy A., Chand N., Barkoula N.M. and Biswas S. (2010) Solid particle erosion wear characteristics of fiber and particulate filled polymer composites: A review, Wear, Vol. 268, p: 249-263.

Yerramareddy S. and Bahadur S.(1991) Effect of operational variables, microstructure and mechanical properties on the erosion of Ti-6Al-4V, Wear, Vol 142, p: 253-263.